Science of the Total Environment 696 (2019) 134076

Contents lists available at ScienceDirect

Science of the Total Environment

journal homepage: www.elsevier.com/locate/scitotenv

Projecting meteorological, hydrological and agricultural droughts for the Yangtze River basin

Fengyun Sun [a,b,c,d], Alfonso Mejia [d], Peng Zeng [a,b,c], Yue Che [a,b,c,*]

[a] School of Ecological and Environmental Sciences, East China Normal University, Shanghai 200241, China
[b] Shanghai Key Lab for Urban Ecological Processes and Eco-Restoration, East China Normal University, Shanghai 200241, China
[c] Institute of Eco-Chongming (IEC), Shanghai 200062, China
[d] Department of Civil and Environmental Engineering, The Pennsylvania State University, University Park, PA 16802, USA

HIGHLIGHTS

- The raw CMIP5 ensemble overestimates precipitation while underestimating temperature for the Yangtze River basin.
- Precipitation, runoff and soil moisture were all projected to increase in the coming decades.
- Drought magnitude was anticipated to shift from moderate and severe in the past to extreme and exceptional in the future.
- Agriculture drought was projected to be more severe than meteorological and hydrological droughts.
- The headwater areas were anticipated to increase in Agriculture drought severity.

GRAPHICAL ABSTRACT

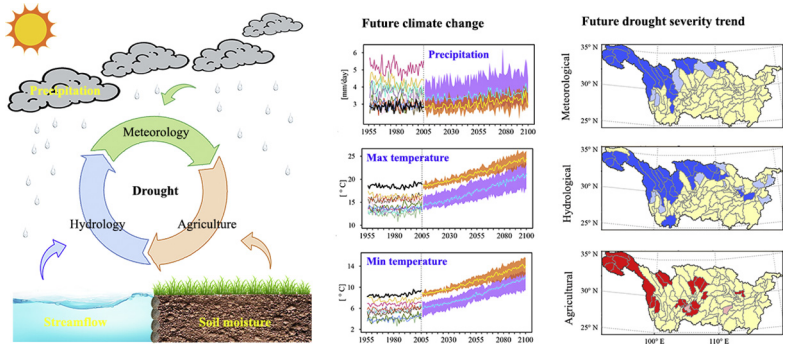

ARTICLE INFO

Article history:
Received 10 January 2019
Received in revised form 21 August 2019
Accepted 22 August 2019
Available online 23 August 2019

Editor: Ralf Ludwig

Keywords:
Drought prediction
Drought index
CMIP5
RCP emission scenarios
Statistical downscaling
SWAT

ABSTRACT

Drought is a multifaceted natural hazard that occurs in virtually any component of the hydrological cycle. Drought monitoring and prediction from multiple viewpoints are essential for reliable risk planning and management. This study presents a joint prognosis of meteorological (M-drought), hydrological (H-drought) and agricultural (A-drought) droughts for the period 2021–2100 over the Yangtze River basin (YRB). The prognosis uses an ensemble of 10 models from the Coupled Model Intercomparison Project Phase 5 (CMIP5) for two future emission scenarios (RCP4.5 and RCP8.5). Precipitation, runoff, and soil moisture are used to quantify M-drought, H-drought, and A-drought, respectively. The results indicate that the raw CMIP5 multimodel ensemble for the YRB generally overestimates precipitation while underestimating temperature. The precipitation, runoff, and soil moisture are all projected to increase in the coming decades at the spatial scale of the entire YRB. Moreover, the magnitudes of drought shift from moderate and severe in the past (1954–2013) to extreme and exceptional in the future. The durations of drought are anticipated to prolong in the future, especially for the A-droughts. A-droughts are projected to be more severe than M- and H-droughts. Furthermore, the headwater areas and the areas surrounding the intersection of Sichuan, Guizhou and Chongqing are anticipated to increase in A-drought severity. These findings provide insight to inform drought planning and management in the YRB, and improve our understanding of the ability of precipitation, runoff, and soil moisture to describe droughts under global warming scenarios.

* Corresponding author at: School of Ecological and Environmental Sciences, East China Normal University, Shanghai 200241, China.
E-mail address: yche@des.ecnu.edu.cn (Y. Che).

https://doi.org/10.1016/j.scitotenv.2019.134076
0048-9697/

1. Introduction

Droughts are a recurring natural hazard that can occur in virtually all parts of the world (Rajsekhar and Gorelick, 2017; Schwalm et al., 2017). Droughts are capable of resulting in substantial ecological (Schwalm et al., 2017; Vicca et al., 2016) and socioeconomic (Touma et al., 2015) impacts. Thus, there is great scientific and societal interest in accurately understanding future drought trends, particularly since global warming could make drought conditions worse in many regions around the world (Cook et al., 2015; Dai, 2011). Ultimately, understanding future drought conditions is necessary to regional, national, and global food, energy, and water security. Drought conditions can severely affect regional crop production (Lesk et al., 2016; Sehgal et al., 2017), which can lead to food shortages and, in some extreme cases, famine, further triggering or exacerbating human conflict and involuntary migration in vulnerable populations. Droughts can threaten water supplies (artificial reservoirs and natural sources such as groundwater) (Nazareno and Laurance, 2015), affecting cities worldwide and undermining our ability to rely on hydropower for electricity production. The World Economic Forum (2017) consistently ranks environmental risks associated with extreme weather events, water crises, and climate change at the top of their list of global risks facing humanity now and into the future. Australia's Millennium Drought (Van Dijk et al., 2013) and the multiyear California drought (Griffin and Anchukaitis, 2014) are two vivid examples of the impacts of droughts.

When examining historical observations since 1950, drought trends across the globe are diverse, consisting of a mixture of drying and wetting regions (Sheffield et al., 2012). For instance, it seems likely that drought severity and frequency have increased in the Mediterranean and West Africa, and decreased in central North America and northwest Australia (Kirtman et al., 2013). In the case of China, drought trends vary substantially within the country (Dai, 2011; Sheffield et al., 2012; Zou et al., 2005). Based on global drought assessments, the general tendency since 1950 shows a significant drying trend in northern China, while a slight drying trend in the southern region and a slight wetting trend in most of the eastern region (Dai, 2011; Sheffield et al., 2012). In contrast, regional drought analyses reveal that severe and frequent droughts can occur throughout most of China (Lu et al., 2011; Wang et al., 2011; Xu et al., 2015; Yang et al., 2012). Indeed, drought is a critical concern in China because of its large country area and population, extensive agricultural sector, dependence on hydroelectric power use (main energy source after coal and oil), and fast growing urbanization and economy. Droughts are a major cause of economic loss in China, ~35% of all losses from natural disasters (Song et al., 2003).

The Yangtze River basin (YRB) in China is of primary importance because of its water resources endowment and economic productivity. The YRB occupies nearly 20% of China's land area (Guan et al., 2015) but accounts for over 36% of its water resources (Liu et al., 2016), accommodates nearly 33% of its population, and contributes about 40% of its total GDP (Gao et al., 2012). Several studies have shown, using historical observations, that changing drought frequency and severity in the YRB are an important and significant concern. For instance, studies indicate that drought frequency increased in the middle area of the YRB (Gemmer et al., 2008; Zhai et al., 2010) during the period 1960–2005. During this same period, trends have also been found in other parts of the YRB. Zhai et al. (2010) found a significant decreasing trend in drought frequency in the upper and lower YRB, while Xu et al. (2015) and Zhou et al. (2017) have shown increasing trends in the southern part of the YRB.

With knowledge of significant drought trends in the YRB's near past, the question arises as to how will these trends be affected by projected changes in climate. Studies based on outputs from the Coupled Model Intercomparison Project Phase 3 (CMIP3) indicate that projected droughts will increase in frequency and severity in China (Leng et al., 2015). Furthermore, using CMIP5 outputs, several studies have highlighted the potential for droughts to worsen in the YRB. Lu et al. (2016) projected that droughts in the upstream YRB during 2021–2050 would be more frequent and severe compared to 1971–2000. Wang and Chen (2014) predicted, using the Palmer Drought Severity Index (PDSI), a dramatic increase in severe and extreme droughts in the west part of the YRB. Several other studies have used CMIP5 outputs to explore future climate change in the YRB (Deng et al., 2013; Pan et al., 2016; Wu et al., 2016). These studies, however, have not been performed at the subbasin level, which are spatial units relevant to water-related decision- and policy-making, and have mostly relied on a single drought variable to assess drought conditions. We perform here for the first time a comprehensive multivariable analysis of projected droughts in the YRB at the subbasin level.

Droughts can be defined in different ways. They are commonly defined according to the following four different types: i) meteorological drought (M-drought), which is based on the lack of precipitation over a region for a period of time (Mishra and Singh, 2010); ii) hydrological drought (H-drought) is defined as a period over which water supply is low in streams, reservoirs, and/or groundwater (Dracup et al., 1980); iii) agricultural drought (A-drought) is characterized by a period with declining soil moisture and consequent crop failure (Dracup et al., 1980); and iv) socioeconomic drought is related to the impact of drought conditions on the supply and demand of an economic commodity (Mishra and Singh, 2010). To quantify droughts according to these four types, a number of indices have been developed and implemented. Multivariate drought indices that incorporate multiple drought information into one measurable indicator are often employed. Comprehensive reviews of commonly used drought indices are available elsewhere, e.g., Dai (2011), Hao and Singh (2015), Heim (2002), and Mishra and Singh (2010). A popular approach is to use standardized indices (SI) (McKee et al., 1993; Shukla and Wood, 2008; Vicente-Serrano et al., 2010), which transform a drought relevant variable, or joint variables, into a standardized measure. This facilitates interpretability by being independent of units and comparability across regions by using a common standard.

The selection of an appropriate index is a crucial step in performing drought assessments (Farahmand and AghaKouchak, 2015; Guttman, 1999; McKee et al., 1993; Shukla and Wood, 2008; Thilakarathne and Sridhar, 2017). When employing different variables to quantify droughts, it becomes particularly important to use a consistent statistical technique to obtain the indices, avoid making conflicting statistical assumptions, and ensure comparability. Here we use the generalized SI approach recently developed by Farahmand and AghaKouchak (2015). This approach is desirable because it uses the same empirically-based, non-parametric distribution, namely the Gringorten plotting position (Gringorten, 1963), to derive different indices (AghaKouchak, 2014; Kang and Sridhar, 2017; Nasrollahi et al., 2015). Specifically, we use the approach by Farahmand and AghaKouchak (2015) to obtain the following three drought indices: i) standardized precipitation index (SPI) (McKee et al., 1993) for M-drought, ii) standardized runoff index (SRI) (Shukla and Wood, 2008) for H-drought, and iii) standardized soil moisture index (SSI) (AghaKouchak, 2014) for A-drought.

Our primary goal with this study is to perform at the subbasin level a multivariable drought assessment of the YRB using projected precipitation, runoff, and soil moisture ensembles over the period 2021–2100. To this end, we force a semidistributed hydrological model, namely the Soil and Water Assessment Tool (SWAT) (Arnold et al., 1998), with downscaled outputs from 10 different CMIP5 models and 2 different emission scenarios. We then use the downscaled CMIP5 and hydrological model outputs to obtain precipitation, runoff, and soil moisture and compute the SPI, SRI, and SSI, respectively, across 125 different subbasins in the YRB. To downscale the precipitation and temperature CMIP5 outputs, we use a modified version of the daily bias-corrected spatial disaggregation (BCSD) method (Girvetz et al., 2013; Wood et al., 2002; Wood et al., 2004).

This study is more comprehensive than previous drought assessments for the YRB, differing in the following key aspects. We employ three different indices to perform the drought assessment, whereas previous studies have tended to emphasize a single index. Moreover, we use a common statistical approach to obtain the different indices, avoiding potential statistical inconsistencies among the indices. In contrast with previous studies for the YRB, the drought assessment is performed at the subbasin level. Additionally, we use projected runoff and soil moisture to determine drought conditions, whereas past studies have mostly relied on downscaled climate variables such as precipitation. Some of the questions motivating this study are as follows: What are the likely and dominant drought trends in the YRB for the 21st century? Do the multimodel ensemble members agree on the direction of drought trends? How do these trends vary among subbasins in the YRB? How consistent are the different indices with respect to each other in projecting droughts?

2. Study area

Our study area consists of the YRB (Fig. 1), also known as the Changjiang basin. We select the YRB since it is one of the largest basin in the world, which contributes significantly to both the Chinese and global economy through export products that are directly or indirectly supported by its water resources. The YRB drains at the mouth an area of ~1.8 million km^2. Owing to its sheer size, the YRB is comprised of a spatially diverse climate, hydrology, pedology, physiography, and land cover. The long-term annual precipitation ranges from 500 mm in the West to 2500 mm in the East, with an average of ~1070 mm. The land cover in the YRB consists primarily of forests (43.8%), agricultural areas (28.5%) and grasslands (22.1%), some less dominant land cover types are water bodies (1.9%), shrublands (1.4%) and urban areas (1.3%) (Sun et al., 2016). Further information about the physiographic and hydroclimatological characteristics of the YRB can be found elsewhere e.g., Gao et al. (2012), Guan et al. (2015), and Sun et al. (2016).

3. Datasets

3.1. CMIP5 precipitation and temperature

We use daily CMIP5 precipitation and max/min temperature to force the hydrological model SWAT and obtain projected daily runoff and soil moisture across subbasins in the YRB over the period 2021–2100. The daily precipitation and max/min temperature outputs are obtained for 10 different CMIP5 models to consider uncertainty and inter-model variability. The selected climate models are: ACCESS1-3, GFDL-CM3, GFDL-ESM2G, GFDL-ESM2M, IPSL-CM5A-LR, IPSL-CM5A-MR, MIROC5, MRI-CGCM3, MIROC-ESM, and MIROC-ESM-CHEM. These models are selected because their capabilities are well-documented and are known to perform well (Nasrollahi et al., 2015; Orlowsky and Seneviratne, 2013; Venkataraman et al., 2016). For each model, the following two Representative Concentration Pathway (RCP) scenarios are considered: i) RCP4.5, which is a midrange mitigation emissions scenario with radiative forcing stabilized at ~4.5 W/m^2 before 2100; and ii) RCP8.5, which is a high emissions scenario with radiative forcing >8.5 W/m^2 by 2100 (Moss et al., 2010). These two scenarios are within the core set of the CMIP5 runs and are recommended as a first priority for assessment studies (Taylor et al., 2012).

3.2. Data required by the hydrological model

Studies have successfully employed SWAT and CMIP5 to project long-term streamflow or soil moisture in basins worldwide (Basheer

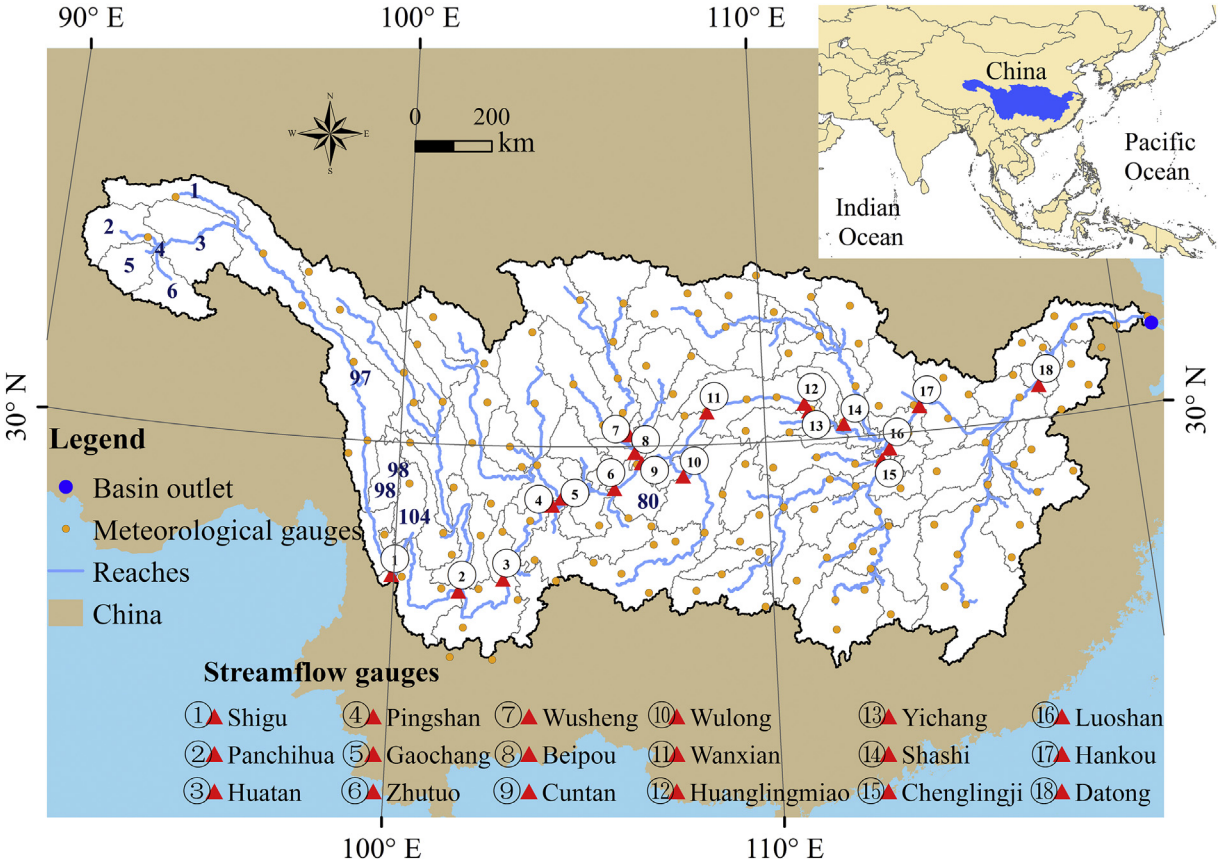

Fig. 1. Map illustrating the boundary, 125 subbasins, meteorological and streamflow gauges of the Yangtze River basin (YRB). The legend highlights the subbasins and daily streamflow gauges used to calibrate/validate the hydrological model. Several subbasins mentioned in the text are labeled. The inset shows the location of the YRB within China and East Asia.

et al., 2016; Shrestha et al., 2017; Tan et al., 2017). We use the SWAT model to project runoff and soil moisture in the YRB over the period 2021–2100. The SWAT model employed was previously developed and calibrated on a monthly time step to study historical hydrological conditions in the YRB (Sun et al., 2016). Here we further improve this SWAT model by calibrating it to daily observations. To configure the SWAT model, precipitation and max/min temperature observations, digital soil, land cover, and terrain data are used. Precipitation and max/min temperature are characterized using 148 daily meteorological stations from the National Meteorological Information Center (http://data.cma.cn/). Soils are characterized using the two-layer Harmonized World Soil Database of the FAO (http://www.fao.org/soils-portal/soil-survey/soil-maps-and-databases/en/), which includes for the YRB 96 different soil types and their main physical properties. Land cover is characterized using the GlobeLand30 (http://www.globallandcover.com) dataset, which is for the year 2010 with a 1 arc-second grid spatial resolution. Terrain is characterized using Advanced Spaceborne Thermal Emission and Reflection Radiometer data (http://www.jspacesystems.or.jp) with a 1 arc-second grid of elevation postings. To calibrate and validate the SWAT model, daily observations from 18 streamflow gauges are used (Fig. 1). The streamflow data are obtained from the Changjiang River Water Resources Commission (http://www.cjh.com.cn/). Further details about the performance of the SWAT model are included in the methodology section (Section 4).

4. Methodology

This section describes the methodology followed to perform the multivariable drought assessment of the YRB. An overview of the datasets, approaches, and interdependence among different components of the methodology is provided in the flow diagram in Fig. 2.

4.1. CMIP5 downscaling

A critical step in using global climate projection data while emphasizing regional detection is to postprocess, i.e. downscale and bias correct, the data. A number of statistical downscaling methods have been developed for various research purposes and applications. The BCSD method (Wood et al., 2002; Wood et al., 2004) is widely used to spatially disaggregate and bias-correct monthly CMIP5 outputs. We employ a modified version of the BCSD suitable for handling daily projections (Girvetz et al., 2013). The approach is described next.

To spatially downscale the climate projections, the gridded CMIP5 precipitation and temperature data are linearly interpolated onto the 148 individual weather stations in the YRB (Fig. 1). To bias-correct the climate projections, each data point in 2006–2100 is mapped onto the cumulative distribution function (CDF) of the historical CMIP5 data first and then the resulting value is mapped onto the inverse CDF of the historical observations (Gudmundsson et al., 2012; Jakob Themeßl

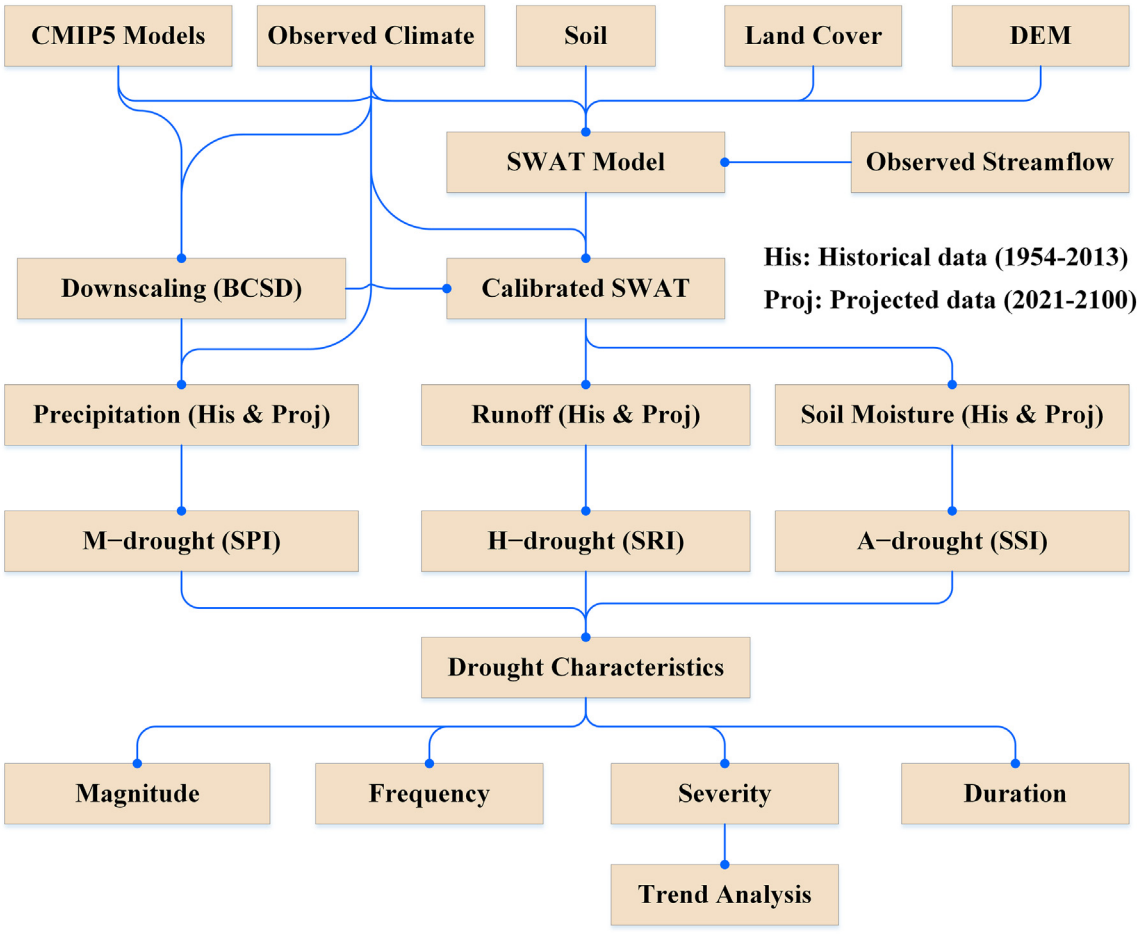

Fig. 2. Schematic diagram illustrating the overall methodology followed in this study to perform the multivariable drought assessment of the YRB. At the top, the methodology begins by assembling the necessary digital data to perform the climate downscaling and configure/calibrate the SWAT model. The data include the CMIP5 outputs, as well as observed precipitation, temperature, streamflow, digital soil, land cover, and terrain information. The CMIP5 precipitation and temperature data are downscaled using observations from the period 1954–2013 as reference. In the next step of the methodology, the calibrated SWAT model is forced with the downscaled CMIP5 precipitation and temperature data to generate projected runoff and soil moisture for the period 2021–2100. The downscaled precipitation, and the projected runoff and soil moisture are then used to compute the SPI, SRI, and SSI, respectively, for 125 subbasins covering the YRB. Lastly, to characterize drought conditions, we analyze each index using different drought characteristics such as the magnitude, frequency, severity, and duration. We further analyze the severity to assess drought trends using the Mann-Kendall method.

et al., 2011; Wang and Chen, 2014). A moving window of ±15 days (Thrasher et al., 2012) around the date of the data point in 1954–2005 is used to construct the CDFs. Empirical distributions are adopted to fit the CDFs (Gudmundsson et al., 2012). Note that to preserve the potential long-term trend in the climate projections and avoid potential deterioration of the quantile mapping (Maraun, 2016; Teutschbein and Seibert, 2012), we remove the trend before bias correcting the raw outputs and then add it back after the bias correction is performed (Girvetz et al., 2013). To handle any outliers in the empirical CDFs, we follow the procedure of (Boé et al., 2007). The downscaling is done for the 10 selected CMIP5 models for the RCP4.5 and RCP8.5 scenarios.

4.2. Hydrological model

We force the calibrated SWAT model with the downscaled CMIP5 precipitation and temperature outputs to project runoff and soil moisture over the period 2021–2100. SWAT is a spatially semidistributed hydrological model that accounts for main hydrological processes in each spatial modeling unit or subbasin. We divide the YRB into 125 subbasins (Fig. 1), the median subbasin area is ~11,191 km^2. The hydrologic processes simulated by SWAT include canopy storage, soil infiltration, redistribution of water within the soil profile, evapotranspiration, lateral subsurface flow, surface runoff, ponds, channel flow, and return flow (Arnold et al., 2012). In SWAT, after precipitation reaches the soil surface, it may infiltrate into the soil profile or generate runoff. Infiltrated water may be held in the soil and later evapotranspired, or it may slowly make its way to the surface-water system via groundwater flow. Snow is computed when temperatures are below freezing. Precipitation is classified as rain or snow based on the average daily temperature. Snow melt is controlled by the air temperature, snow pack temperature, the melting rate, and the snow areal coverage. Melted snow is treated the same as rainfall for estimating runoff and percolation. Within SWAT, we use the SCS curve number, the Priestley-Taylor method, and the variable storage coefficient method to model surface runoff, potential evapotranspiration, and channel flow routing, respectively. A kinematic storage model is used to model lateral flow in each soil layer.

The performance of the calibrated SWAT model is evaluated at the 18 hydrological stations in the YRB, each station with 21-year long consecutive daily discharge observations. Although the temporal resolution of this study is monthly, the SWAT model is calibrated and validated using daily observations to improve model accuracy. The calibration and validation period are 15 years (Jan. 1st 1990–Dec. 31st 2004) and 6 years (Jan. 1st 2005–Dec. 31st 2010), respectively. To assess the performance of the SWAT model, the coefficient of determination, R^2, and the Nash-Sutcliffe coefficient, NS, are used (Table 1). Overall, the model performs reasonably well with median R^2 and NS values of 0.84 and 0.71, respectively, for the combined calibration and validation period (1990–2010). Thus, the model is deemed suitable for investigating the impacts on droughts of climate projections in the YRB.

Table 1
Summary of the SWAT model performance. Note that the gauge numbers in the table correspond to the gauge locations shown in Fig. 1.

Streamflow gauge name	Gauge no.	Calibration		Validation	
		R^2	NS	R^2	NS
Shigu	1	0.71	0.32	0.84	0.68
Panzhihua	2	0.80	0.67	0.85	0.74
Huatan	3	0.88	0.67	0.90	0.68
Pingshan	4	0.88	0.70	0.90	0.70
Gaochang	5	0.61	0.47	0.62	0.43
Zhutuo	6	0.83	0.72	0.87	0.72
Wusheng	7	0.44	0.41	0.55	0.55
Beipou	8	0.49	0.48	0.53	0.53
Cuntan	9	0.83	0.77	0.82	0.76
Wulong	10	0.52	0.46	0.57	0.40
Wanxian	11	0.84	0.78	0.84	0.79
Huanglingmiao	12	0.85	0.84	0.79	0.74
Yichang	13	0.86	0.81	0.79	0.74
Shashi	14	0.87	0.83	0.81	0.70
Chenglingji	15	0.63	0.61	0.62	0.60
Luoshan	16	0.89	0.87	0.87	0.80
Hankou	17	0.90	0.89	0.88	0.86
Datong	18	0.86	0.83	0.86	0.83

4.3. Standardized drought indices

We use the downscaled CMIP5 monthly precipitation to calculate the SPI, and the projected monthly runoff and soil moisture from the SWAT model to compute the SRI and SSI, respectively. Note that the SPI, SRI, and SSI are used to represent M-drought, H-drought, and A-drought, respectively. Monthly precipitation, runoff, and soil moisture are estimated for each subbasin. Specifically, precipitation for a single subbasin is the monthly average precipitation falling on the subbasin area during a given month. Runoff is the monthly net average amount of water that leaves the subbasin area to a river reach. Soil moisture is the monthly average amount of water in the soil profile of a subbasin area within a maximum depth of 100 cm from the top of the soil.

To obtain the indices for the historical period, we follow the approach by Farahmand and AghaKouchak (2015). For this, we let $x(t)$ represent the monthly data at time t. For a given n-month timescale (e.g., *3*-, *6*-, or *12*-months), the accumulated variable $X_n(t)$ is calculated as follows:

$$X_n(t) = \sum_{t-n+1}^{t} x(t). \quad (1)$$

The time series $X_n(t)$ is then subdivided into subseries $S_n(m)$ with respect to a particular month m such that

$$S_n(m) = [X_n(m), X_n(1 \times 12 + m), \ldots, X_n((N-1) \times 12 + m)] \quad (2)$$

where $m = 1, 2, \ldots, 12$ represents the calendar months, and N is the number of years considered. The empirical Gringorten plotting position is used to compute the cumulative frequency of $S_n(m)$ as follows:

$$P_{nm}(i) = \frac{i_{nm} - 0.44}{N + 0.12} \quad (3)$$

where i_{nm} denotes the rank of $S_n(m)$ from the smallest to the highest, and $P_{nm}(i)$ is the estimate of the cumulative frequency of the ith term in the month m. The empirical probabilities are transformed into the standard normal distribution function according to

$$SI_{nm} = \Phi^{-1}(P_{nm}) \quad (4)$$

where SI_{nm} denotes the standardized index for month m and timescale n, and Φ denotes the standard normal distribution function (AghaKouchak, 2014; Farahmand and AghaKouchak, 2015).

Note that in this case the SI_{nm} is equal to SPI, SRI, or SSI when $x(t)$ is set equal to precipitation, runoff, or soil moisture, respectively. The timescale n is selected depending on the research and user needs, and scales of 3-, 6-, and 12-months are commonly adopted (Orlowsky and Seneviratne, 2013). Short-term durations spanning a few months may be particularly relevant to meteorological (Vicente-Serrano et al., 2010) and agricultural (Guttman, 1999) applications, while long-term durations may be relevant for water supply management purposes (Heim, 2002). We use a 3-month duration since both meteorological and agricultural droughts are an important concern in the YRB.

To compute the SI_{nm} values for the projected precipitation, runoff, and soil moisture data in the period 2021–2100, we use the mapping between the values of $S_n(m)$ and SI_{nm} for the baseline (historical) period (1954–2013). That is, the SI_{nm} values for the projected data are determined in reference to the historical SI_{nm} values. In this way, for example,

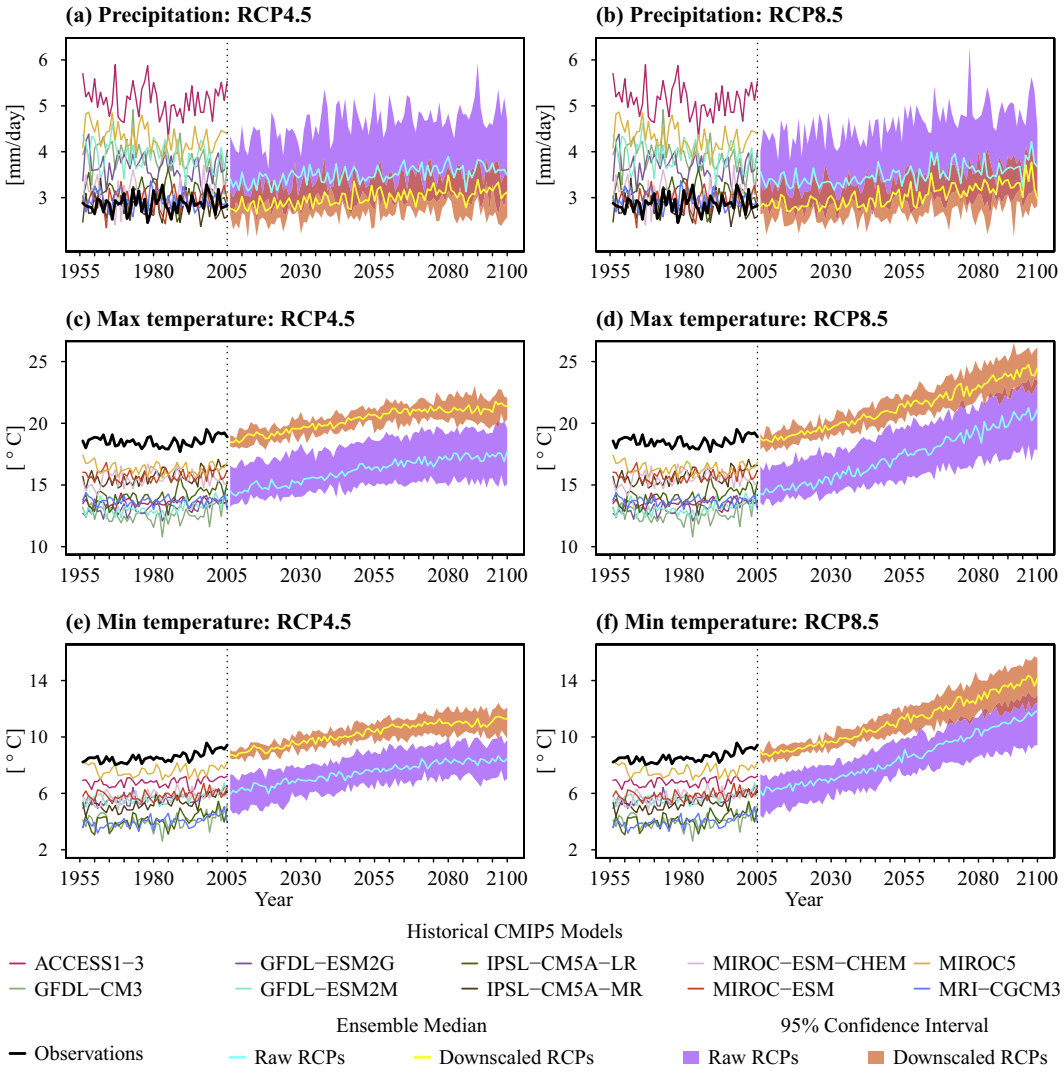

Fig. 3. Performance of the areal averaged, downscaled, daily a–b) precipitation, c–d) maximum temperature, and e–f) minimum temperature for the RCP4.5 and RCP8.5 scenarios, respectively, over the YRB. For the historical period (1954–2005), the observed values are shown (black line) together with the historical projections from each of the 10 selected CMIP5 models. For the future projected period (2006–2100), the raw and downscaled ensemble median, together with their corresponding 95% confidence intervals, are shown.

when an increase in drought severity is identified in the projected data, this increase is relative to the historical drought conditions.

4.4. Drought characteristics

To further characterize droughts in the YRB, the drought indices are used to compute the drought severity, duration, frequency, and magnitude. To compute the drought severity, duration, and frequency, one must first define what a drought event is. Typically, a low statistical threshold or trigger point is used. Thus, we define drought events as a period in which the SI values are continuously below the threshold SI = -0.8, corresponding to ~20% of the time series, which is a commonly used drought threshold (AghaKouchak, 2014; Svoboda et al., 2002). Note that our definition of drought includes the date when the SI first drops below the selected threshold as the beginning, and the date before the SI first climb above the threshold as the end. Accordingly, the drought duration is the number of consecutive months within one drought event; the drought severity is the positive sum of all the SI values within one drought event; and the drought frequency is calculated as the number of drought occurrences within a decade. Additionally, we also compute the drought magnitude based on the drought category for each month following the U.S. Drought Monitor classification (Svoboda et al., 2002). The classification is as follows: D1 (moderate drought, 10–20%), D2 (severe drought, 5–10%), D3 (extreme drought, 2–5%), and D4 (exceptional drought, <2%) (Svoboda et al., 2002).

4.5. Drought trend analysis

Another important aspect of drought assessment is to identify potential trends in the drought characteristics. Thus, trend detection is performed on the drought severity at the subbasin level. The aim with this is to identify regional drought patterns based on the three different SI used in this study. The Mann-Kendall (MK) method (Kendall, 1955; Mann, 1945) is employed for the trend analysis. The MK is a nonparametric method for detecting the significance of monotonic trends in time series data. To summarize our trend analysis results, based on the sign of the trend (MK's tau, τ) and the level of significance (p-value), we classify the results into the following 5 categories (López-Moreno et al., 2011; Westmacott and Burn, 1997): i) strong decreasing trend (−2): $\tau < 0$ and p-value ≤0.05; ii) moderate decreasing trend (−1): $\tau < 0$ and 0.05 < p-value ≤0.1; iii) non-significant trend (0): p-value >0.1; iv) moderate increasing trend (1): $\tau \geq 0$ and 0.05 < p-value ≤0.1; and v) strong increasing trend (2): $\tau \geq 0$ and p-value ≤0.05. Note

that decreasing (negative) trends indicate a wetting tendency while increasing (positive) trends indicate a drying tendency.

5. Results and discussion

5.1. Performance of the downscaled precipitation and temperature CMIP5 outputs

Fig. 3 illustrates the performance of the areal averaged, downscaled, daily CMIP5 precipitation and max/min temperature outputs for the RCP4.5 (left panels) and RCP8.5 (right panels) scenarios. In all the panels in Fig. 3, it can be seen that there is a large bias between the raw CMIP5 outputs (blue line in the period 2006–2100) and the observations (black line in the period 1954–2005). For example, at around the year 2005, the raw CMIP5 max temperature for RCP4.5 (Fig. 3c) is ~14 °C while the historical maximum temperature is ~18 °C. It can also be seen in Fig. 3 that after the BCSD method is applied the bias is largely corrected so that the future projected data (yellow line in the period 2006–2100) aligns well with the observations (black line in the period 1954–2005). For the YRB, the overall bias of the raw CMIP5 outputs is to overestimate precipitation (+0.48 mm/day on average), and underestimate the maximum (−4.04 °C) and minimum (−2.68 °C) temperatures. The panels in Fig. 3 also show that the overall trend in the raw CMIP5 outputs (2006–2100) is preserved after downscaling (yellow line in the period 2006–2100). For instance, the R^2 between the raw and downscaled RCPs is on average equal to ~0.80. Note that in Fig. 3 the historical and future projected periods are defined as 1954–2005 and 2006–2100, respectively, which is how these periods are defined in the CMIP5 dataset. For the remaining figures and results, however, we use the periods 1954–2013 and 2021–2100 to represent the historical and future projected years, respectively. This redefinition captures the period with available observations for the YRB (1954–2013) and the relevant future years (2021–2100).

Fig. 3 also shows the variability of the 10 selected CMIP5 models or ensembles over the historical period (1954–2005); the variability is larger for precipitation (Figs. 3a-b) than max/min temperature (Figs. 3c-f). However, during the historical period, the observed and raw CMIP5 precipitation ensembles tend to overlap with each other for some of the CMIP5 models, whereas in the case of temperature the bias consistently affects all the models. After downscaling, the overall trends for the YRB over the future projected period consist of: i) increase in precipitation of ~0.40 mm/day (+14.35%) and 0.58 mm/day (+20.65%) for RCP4.5 and RCP8.5, respectively; ii) increase in maximum temperature of ~2.95 °C (+15.93%) and 6.17 °C (+32.85%) for RCP4.5 and RCP8.5, respectively; and iii) increase in minimum temperature of ~2.63 °C (+30.03%) and 5.76 °C (+64.33%) for RCP4.5 and 8.5, respectively. These overall trends indicate that the increase in precipitation may be, in some cases, counteracted by enhanced evapotranspiration in the YRB. The trends suggest that, in terms of runoff and soil moisture, both wetting and drying can be expected, depending on the relative difference between the projected increase in precipitation and temperature. The trends support the need to investigate the effects of future climate projections across subbasins of the YRB, as done in this study, to understand how regional landscape conditions at the subbasin level may interact with the future climate to produce different wetting/drying patterns and trends across the YRB.

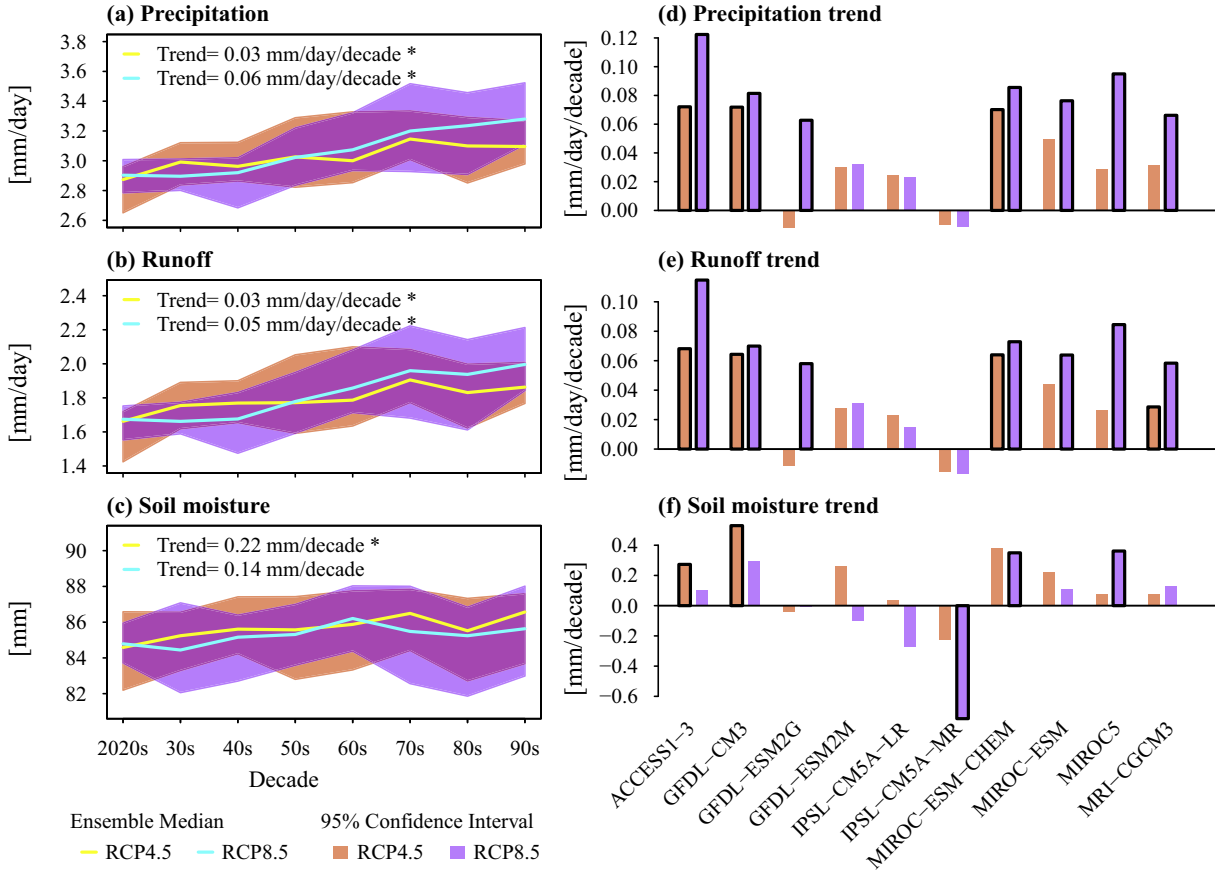

Fig. 4. Projected (2021–2100) decadal variations in the a) precipitation, b) runoff, and c) soil moisture ensemble median for the YRB under the RCP4.5 and RCP8.5 scenarios. The ensemble medians are computed from the areal average over the YRB for each of the 10 selected CMIP5 models. Projected trends in d) precipitation, e) runoff, and f) soil moisture for each of the 10 selected CMIP5 models under the RCP4.5 (in orange) and RCP8.5 (in orchid) scenarios. The trends are assessed over the entire projected period (2021–2100) using linear regression with a 0.05 significance level. In panels d-f, the models with a significant trend are shown using bars with a wider, black delineation.

5.2. Variations in projected precipitation, runoff, and soil moisture

We assess here the overall trend over the entire YRB of the future projected precipitation, runoff, and soil moisture variables, as these trends can have a strong influence on the determination of the different drought types and characteristics. To this end, monthly variables are spatially averaged across the 125 subbasins of the YRB, and are further averaged to a decadal timescale, i.e. the average daily value in a decade. Linear regression is performed on these decadal values to assess changes in precipitation, runoff, and soil moisture at the spatial scale of the entire YRB. We determine the ensemble median associated with each variable over decadal intervals for the future projected period (2021–2100). That is, we compute for every non-overlapping decade in the period 2021–2100 (8 different decades in total) the ensemble median and linear trend associated with the decadal values of precipitation, runoff, and soil moisture.

The decadal variations in the ensemble median over the period 2021–2100 for precipitation, runoff, and soil moisture show an increasing trend (Fig. 4a–c) in the YRB. This is the case for both scenarios, RCP4.5 and RCP8.5. Specifically, we find that the precipitation ensemble median (Fig. 4a) is expected to increase by ~0.03 and 0.06 mm/day/decade under the RCP4.5 and RCP8.5 scenarios, respectively; the runoff ensemble median (Fig. 4b) is expected to increase by ~0.03 and 0.05 mm/day/decade under the RCP4.5 and RCP8.5 scenarios, respectively; and the soil moisture ensemble median (Fig. 4c) is expected to increase by ~0.22 and 0.14 mm/decade under the RCP4.5 and RCP8.5 scenarios, respectively. These trends are all significant at the 5% level, except for the soil moisture ensemble median under the RCP8.5 scenario (Fig. 4c). Thus, the results in Fig. 4a–c indicate that the overall expected trend for the YRB is increased wetting. It is expected that with increasing future precipitation, runoff will also increase in the YRB. Indeed, the average R^2 value between the precipitation and runoff ensembles is 0.96, indicating that the decadal increases in runoff follow closely the precipitation increments. For soil moisture, the wetting trend is less pronounced. Precipitation becomes runoff and soil moisture through the interaction among several governing factors such as temperature, vegetation, land surface properties, and soil composition (Sehgal and Sridhar, 2019). The increasing trend in precipitation has a direct effect on runoff and soil moisture, while the increasing trend in temperature has a counteractive effect. Temperature has a more impactful effect on soil moisture because, with respect to land surface evapotranspiration, soil moisture has a wider and deeper feedback loop than runoff.

This last result can be better illustrated by analyzing the linear trend associated with each of the CMIP5 models considered (Fig. 4d–f) rather than the ensemble median. In the case of precipitation (Fig. 4d) and runoff (Fig. 4e), it can be seen that the trends for the individual models are similar for precipitation and runoff, and the majority of the models agree on the sign of the trend (17 out of the 20 model projections considered, i.e. 10 models × 2 scenarios, show an increasing trend, and out of those 17, 10/11 (precipitation/runoff) show a significant wetting trend). The results are more mixed in the case of soil moisture; 14 out of the 20 model projections show increasing trends and out of those 14, only 4 are significant trends. These results are relevant to the YRB and highlight the need to use different variables and climate models when analyzing droughts. The results show how in terms of soil

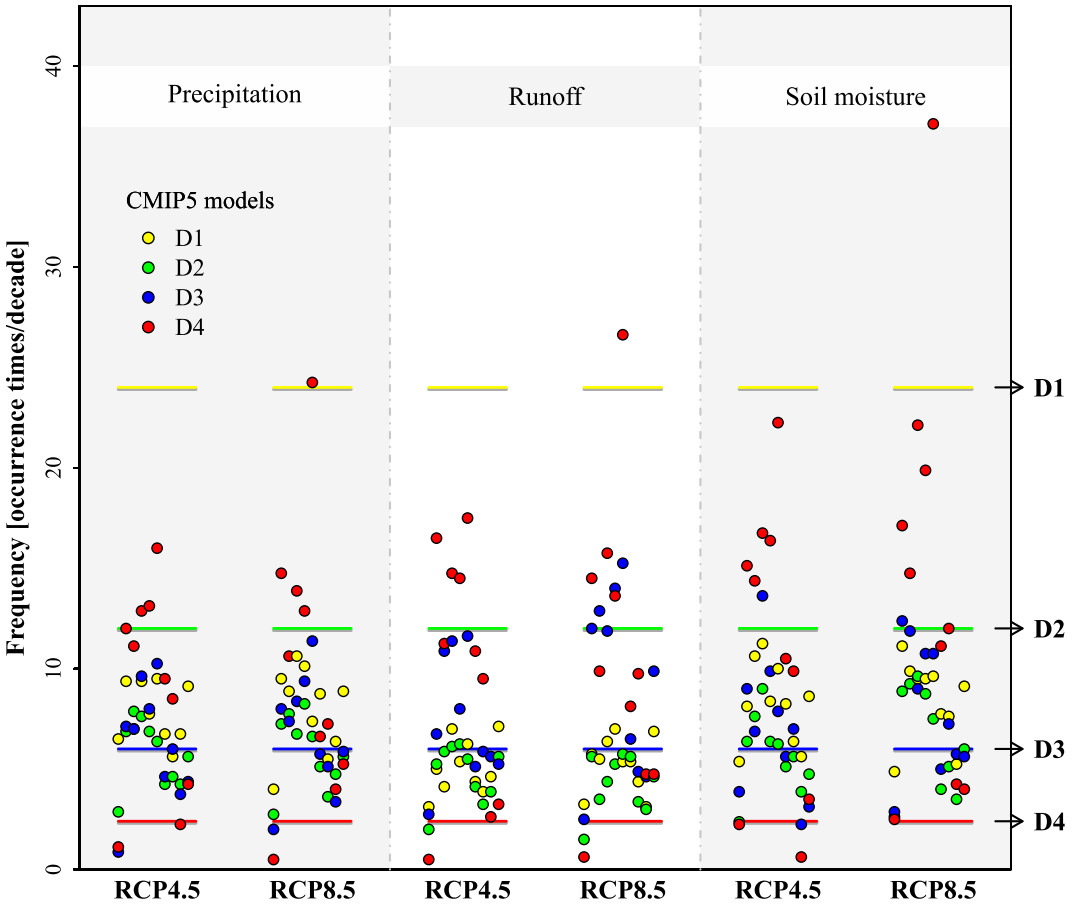

Fig. 5. Classification of future projected (2021–2100) drought frequencies with respect to the baseline, historical period (1954–2013) using the magnitude categories (i.e. D1, D2, D3, and D4) of the U.S. Drought Monitor. The frequency is calculated as the average occurrence time of each drought magnitude in one decade. The classification is done for each of the 10 selected CMIP5 models under both the RCP4.5 and RCP8.5 scenarios. The solid lines indicate the historical frequencies associated with the different drought magnitude categories, while the colored circles represent the future projected values for each of the 10 CMIP5 models.

moisture, which is critical to agricultural activities in the YRB, the wetting trend is weaker than in precipitation and is less consistent across the CMIP5 models. An analysis based only on precipitation trends will tend to miss these potential impacts of climate projections that are of immediate concern to economic activities in the YRB. Now that we have identified the overall trends in the YRB for the variables used to compute the drought indices, we examine next the effect of future projections on the different drought characteristics.

5.3. Comparison between projected and historical drought magnitudes

We use in this subsection drought magnitudes to assess drought conditions over the entire YRB during the future projected period (2021–2100). This drought characteristic is computed for the different drought types considered, i.e., M-drought, H-drought, and A-drought. Recall that the drought indices SPI, SRI, and SSI are used to represent the M-drought, H-drought, and A-drought, respectively, and precipitation, runoff, and soil moisture are used to compute the SPI, SRI, and SSI, respectively.

We find that there are marked differences between the baseline, historical drought magnitudes and the future projected ones for the M-drought, H-drought, and A-drought (Fig. 5). The historical levels for D1, D2, D3 and D4 frequencies are, on average, 24, 12, 6, and 2.4 occurrence times per decade, respectively. While the corresponding levels of mixed scenarios for precipitation are 7.9, 5.8, 6.4 and 9.5, respectively; for runoff are 5.2, 4.5, 8.4 and 10.5, respectively; and for soil moisture are 8.3, 6.1, 7.5 and 12.8, respectively. Specifically, the frequency of moderate, D1, and severe, D2, droughts decreases for the projected data relative to the historical data for all three drought types. This behavior reverses for the extreme, D3, and exceptional, D4, droughts, i.e. D3 and D4 droughts become more frequent in the projected data relative to the historical levels. The increase in D4 frequency is more severe for the A-drought than the M- and H-drought. This is important because it suggests that, according to projected drought trends for the YRB, the agricultural sector may be disproportionately at risk compared to

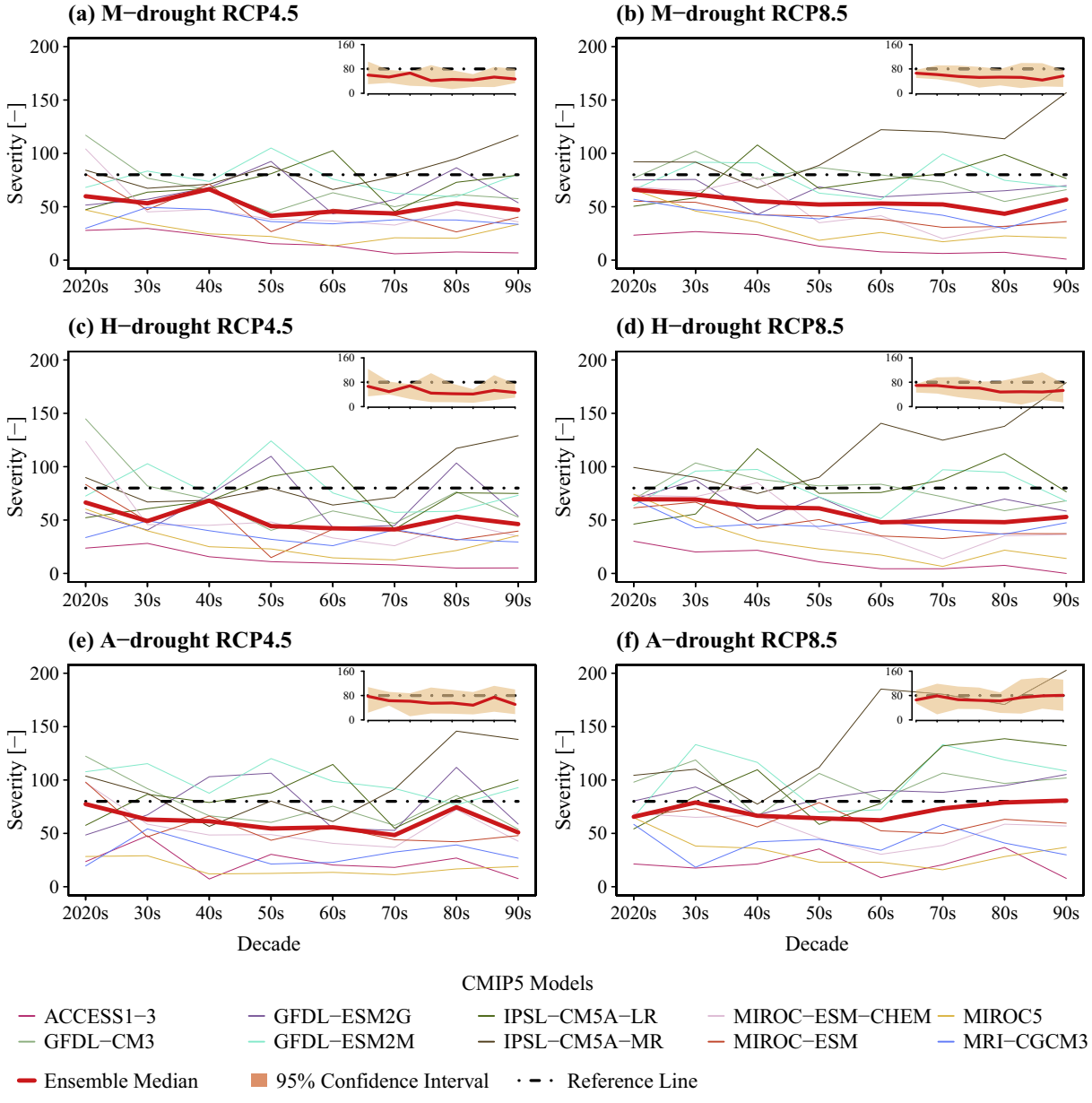

Fig. 6. Projected (2021–2100) decadal variations in drought severity for a–b) M-drought, c–d) H-drought, and e–f) A-drought for the RCP4.5 and RCP8.5 scenarios, respectively. Each panel shows the results for each of the 10 CMIP5 models (thin lines), ensemble median (bold red line), and 95% confidence intervals (shown in the inset). The black dash-dotted line is used as a reference to indicate a horizontal line. (For interpretation of the references to color in this figure legend, the reader is referred to the web version of this article.)

other sectors, such as hydropower and urban water supply, which may be more directly dependent on runoff than soil moisture. Nonetheless, independently of the drought type, the overall tendency during the projected period is for the YRB to shift toward a more severe drought direction (Fig. 5), where moderate droughts are anticipated to decrease while extreme and exceptional ones increase. This shift in drought severity is an important outcome. It suggests the need for future water-related planning in the YRB to account for more frequent extreme drought conditions than implied by historical observations.

5.4. Projected drought characteristics: severity, frequency, and duration

We assess the effect of the projected CMIP5 precipitation and temperature outputs on the severity of the three different drought types over the entire YRB. Recall that severity is computed, in this case, by defining droughts using a threshold of 20% or SI = −0.8. The severity is determined for each drought type in each of the 8 decades in the projected period 2021–2100. We find a decreasing (wetting) temporal trend for the M-drought and H-drought, for both the RCP4.5 and RCP8.5 scenarios (Fig. 6a–d). In the case of the A-drought, the RCP4.5 scenario shows a mild decreasing trend (Fig. 6e), while a slight increasing (drying) trend (Fig. 6f) is only found for the RCP8.5 scenario. Overall, these results indicate a wetting tendency for the entire YRB. This is consistent with our previous results (Fig. 5), which show that moderate and severe droughts are expected to decrease in the YRB.

Another way to assess differences in the drought characteristics over the YRB between the historical and future projected period is by plotting the drought frequency against the average duration (Fig. 7). In particular, for all the three different drought types, we find that the drought durations increase for the future projected period relative to the historical data. For instance, the longest average duration for the A-drought is ~3.5 months for the historical period while for the future projected period the longest duration is ~8.3 months (Fig. 7). In terms of frequency, the behavior of the historical and future projected droughts appears similar. Taken together, these results alongside the ones for the drought magnitude characterization (D1, D2, D3 and D4 in Fig. 5) indicate that, over the YRB, the main effect of the future projected CMIP5 precipitation and temperature outputs is to increase the duration and magnitude (from moderate and severe to extreme and exceptional) of the different drought types.

Comparing the future projected frequency and duration for the different drought types against each other (Fig. 7), the M-drought has the highest frequency but lowest duration, while the H-drought and A-drought are less frequent and prolonged in duration. These differences in the frequency and duration of the three drought types underscore the fact that the variables used to determine the drought types can respond differently to drought conditions. For example, the drought duration is known to vary depending on the variable used to define the drought (Shukla and Wood, 2008; Wilhite and Glantz, 1985; Mo, 2011). In the case of the M-drought, precipitation deficits may develop rapidly, while runoff and soil moisture tend to show a delayed response to precipitation (Entekhabi et al., 1996). In addition, precipitation deficits can end abruptly (e.g., overnight in some cases), while a lag exists between the time an M-drought ends and the time required for the runoff and soil moisture levels to recover from the drought (Heim, 2002; Zhu et al., 2016). Furthermore, a precipitation deficit may not necessarily lead to a runoff or soil moisture deficit (Vicente-Serrano et al., 2011). For example, a short-term, mild-intensity precipitation deficit may

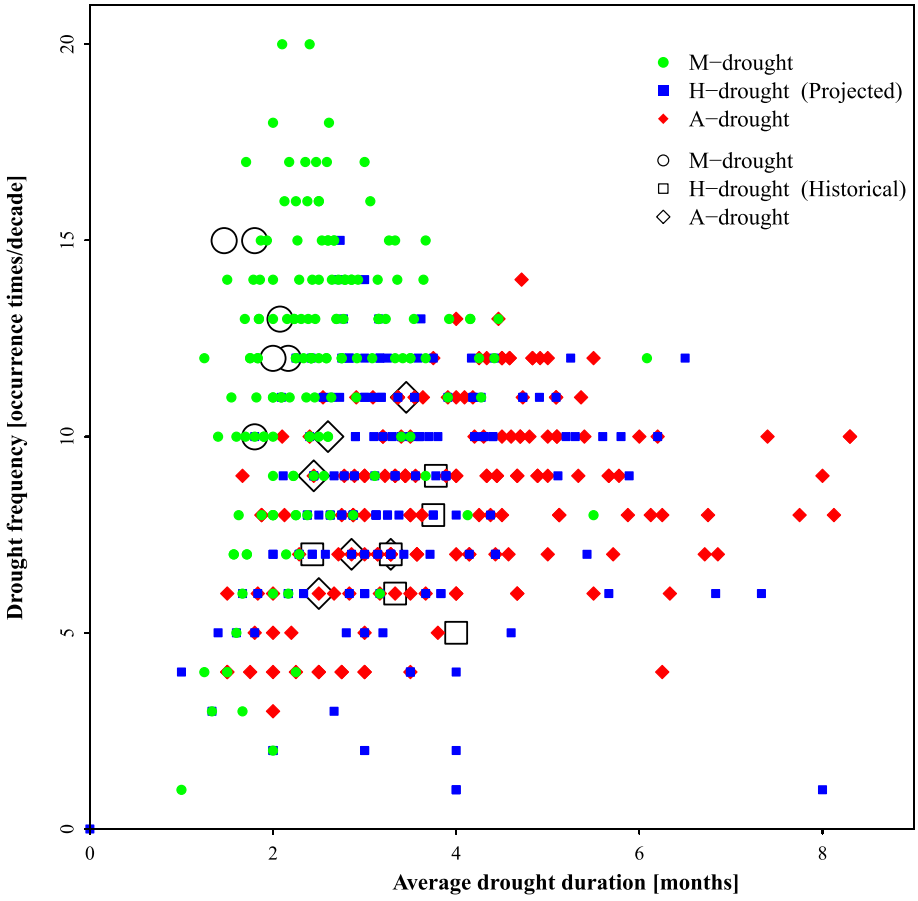

Fig. 7. Plot of the decadal drought frequency against duration for both the historical (1954–2013) and projected (2021–2100) periods. For the historical period, each point in the plot represents the value in a particular decade; the historical period covers 6 different decades. For the projected period, each point represents the value for one of the CMIP5 models in a particular decade. Hence, since 10 models are used over 8 different decades (2021–2100), a total of 80 data points are shown for each drought type.

have little impact on runoff levels in a large river. In summary, our results in Fig. 7 indicate that, in terms of frequency, precipitation is more sensitive in detecting droughts, or can capture the drought onset earlier, than runoff and soil moisture. In terms of duration, runoff and soil moisture capture drought persistence more reliably than precipitation. These drought behaviors for different variables, in terms of frequency and duration, have been reported in a few other studies (e.g., AghaKouchak, 2014; Dracup et al., 1980; Hao and AghaKouchak, 2013) but not for the YRB. The combined analysis of duration and frequency is done for the first time here for the YRB (Fig. 7).

5.5. Spatial patterns of projected drought severity trends

Our previous results provide an integrated assessment of drought conditions for the whole YRB. Further insight, however, can be gained by analyzing droughts at the individual subbasin level, as regional differences, e.g., climate (Bisht et al., 2019), land use (Sehgal and Sridhar, 2018), and topography (Sehgal et al., 2018), can affect drought severity. This is particularly important for the YRB since, due to its sheer size, regional knowledge is needed to inform and enhance drought planning and management. We carry out the MK trend analysis for drought severity in the 125 subbasins of the YRB. Recall that in the MK trend analysis, the values of −2, −1, 0, 1, and 2 indicate strong decreasing, moderate decreasing, non-significant, moderate increasing, and strong increasing trend, respectively. From the spatially explicit MK trend analysis, we find that the trends in most of the subbasins are non-significant (yellow areas) for the M-drought (area ratios of 59.6% and 67.6% for the RCP4.5 and RCP8.5 scenarios, respectively, Fig. 8a–d) and H-drought (area ratios of 49.8% and 57.3% for the RCP4.5 and RCP8.5 scenarios, respectively, Fig. 8b–e). While in the remaining subbasins the trends are all decreasing (blue areas). This is the case for both the RCP4.5 and RCP8.5 scenarios. The A-drought also shows mostly non-significant trends for both scenarios (area ratios of 79.8% and 76.6% for the RCP4.5 and RCP8.5 scenarios, respectively, Fig. 8c–f), but with a few areas revealing a generally increasing trend (red color, area ratios of 12.6% and 23.4% for the RCP4.5 and RCP8.5 scenarios, respectively). The similarity between the spatial patterns of M- and H-drought severity highlight the high correlation and strong causal link between precipitation and runoff. The differences in the spatial patterns of the A-drought, relative to the M- and H-drought, underscore the high importance of evapotranspiration in redistributing water and impacting soil moisture in the YRB.

Figs. 9 and 10 map the trends in drought severity for each of the 10 CMIP5 models across the 125 subbasins of the YRB for scenarios RCP4.5 and RCP8.5, respectively. These figures show the inter-model variability for the different drought types. Overall, both the decreasing trend in M- and H-drought and the increasing trend in A-drought are consistent with the patterns indicated by the multimodel ensemble. The trends in drought severity tend to be more pronounced for the RCP8.5 scenario compared to RCP4.5. Figs. 9 and 10 reveal that projected drought

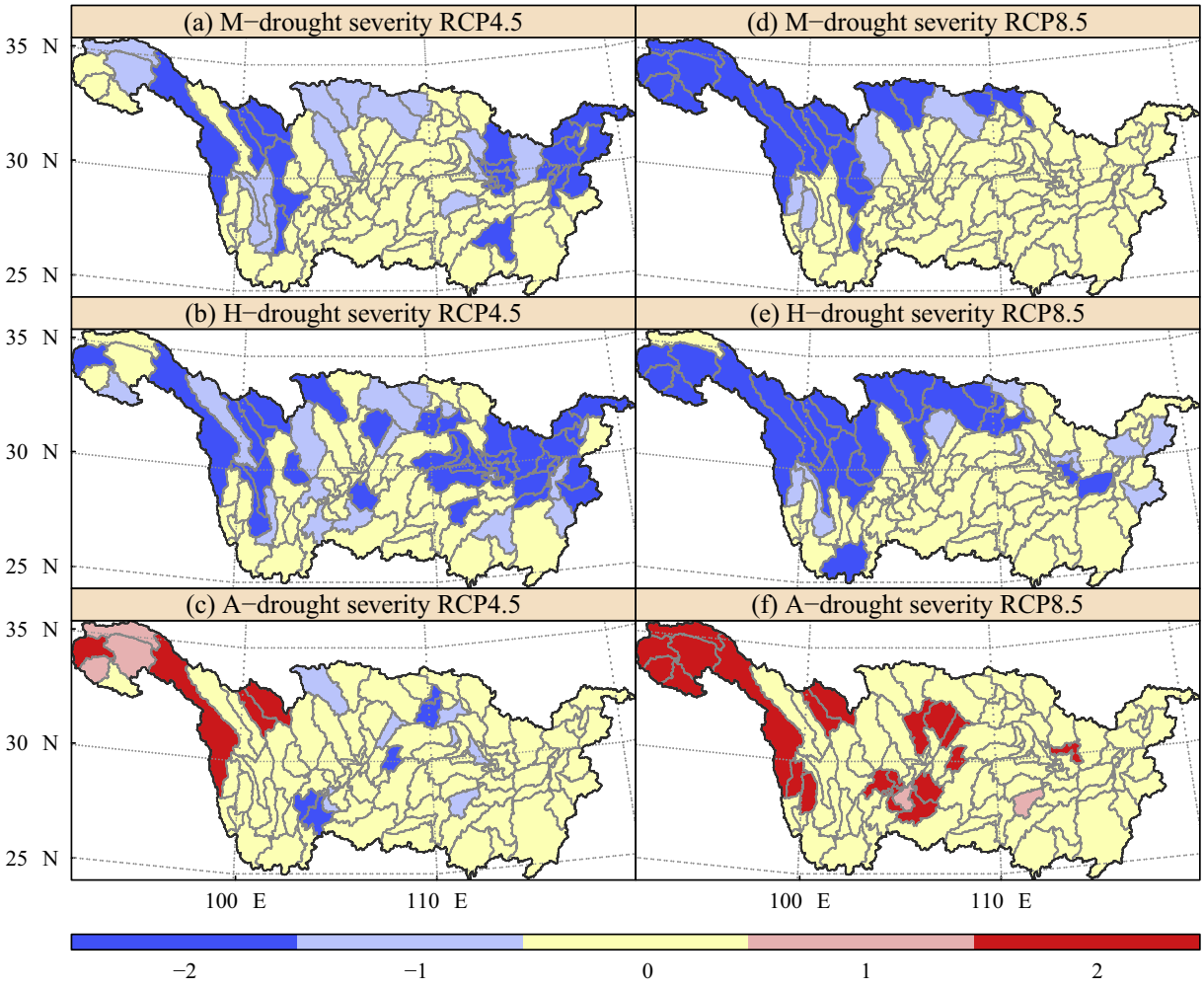

Fig. 8. Projected (2021–2100) spatial variability of drought severity trends in the 125 subbasins comprising the YRB. The trend analysis is performed on the ensemble median of all the CMIP5 models considered. Note that values of −2, −1, 0, 1, and 2 indicate strong decreasing, moderate decreasing, non-significant, moderate increasing, and strong increasing trend, respectively (i.e., increasing positive values indicate a stronger drying trend, while increasing negative ones indicate a wetting trend).

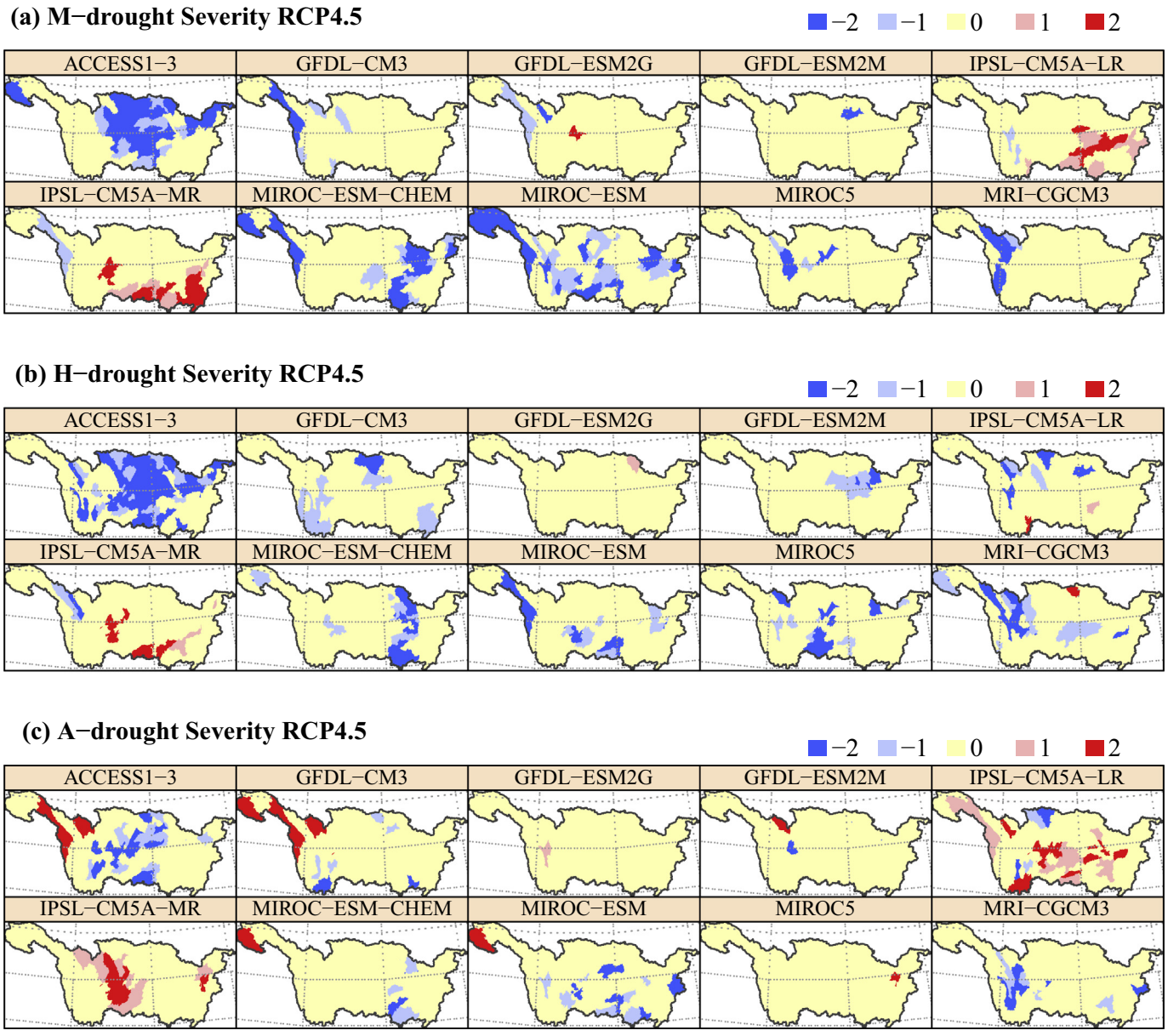

Fig. 9. Map illustrating the MK trend of the individual CMIP5 models for drought severity under the RCP4.5 scenario. Values of −2, −1, 0, 1, and 2 indicate strong decreasing, moderate decreasing, non-significant, moderate increasing, and strong increasing trends, respectively (i.e., increasing positive values indicate a stronger drying trend, while increasing negative ones indicate a wetting trend).

severity can vary widely among the models. For example, area ratios with decreasing trend for the M-drought under the RCP 4.5 scenario can vary from 1.3% (GFDL-ESM2M) to 43.8% (ACCESS1-3) among all the 10 models; and area ratios with increasing trend for the A-drought under the RCP8.5 scenario can vary from 4.2% (MIROC5) to 74.2% (IPSL-CM5A-MR). Despite this variability, consistent patterns can be identified for some areas in the YRB, where the effect of biophysical heterogeneities can be seen to interact with the CMIP5 projections to define drought conditions. Based on this, we identify next geographic regions in the YRB that could benefit from drought planning that incorporates projected information.

The headwater areas (near the Tibetan Plateau) of the YRB, roughly defined as subbasins 1, 2, 3, 4, 5, 6, 97, 98 and 104 (Fig. 1), tend to show an increasing (drying) A-drought trend, and a decreasing (wetting) M-drought and H-drought trend. Unfavorable biophysical conditions, including high elevations, steep slope gradients, shallow land cover, and gravelly soils, make these headwater areas susceptible to aggravated A-droughts. The high elevations and steep slope gradients result in rapid runoff drainage. The dominant land cover in these headwater areas is grassland, which has shallow root depth with relatively low ability to hold and store water. Additionally, the main soil type in these headwater areas is Leptosol, which favors lower soil moisture levels due to this soil's gravelly form, with continuous rock at or very close to the surface (FAO, 2014), and high infiltration rates. All of these conditions could exacerbate droughts in this region. By acting early in the implementation of drought management, some of the negative consequences of future droughts could be prevented.

Another region is the area around subbasin 80 (Fig. 1), where 6 out of the 10 models for the RCP8.5 scenario project an increasing A-drought severity (Fig. 10). This area approximately covers the boundary between two Chinese provinces (Sichuan and Guizhou) and the area in one province-level municipality (Chongqing). This area is one of the most developed areas in the YRB, where future drought impacts could result in substantial economic losses. For example, the Chengdu plain

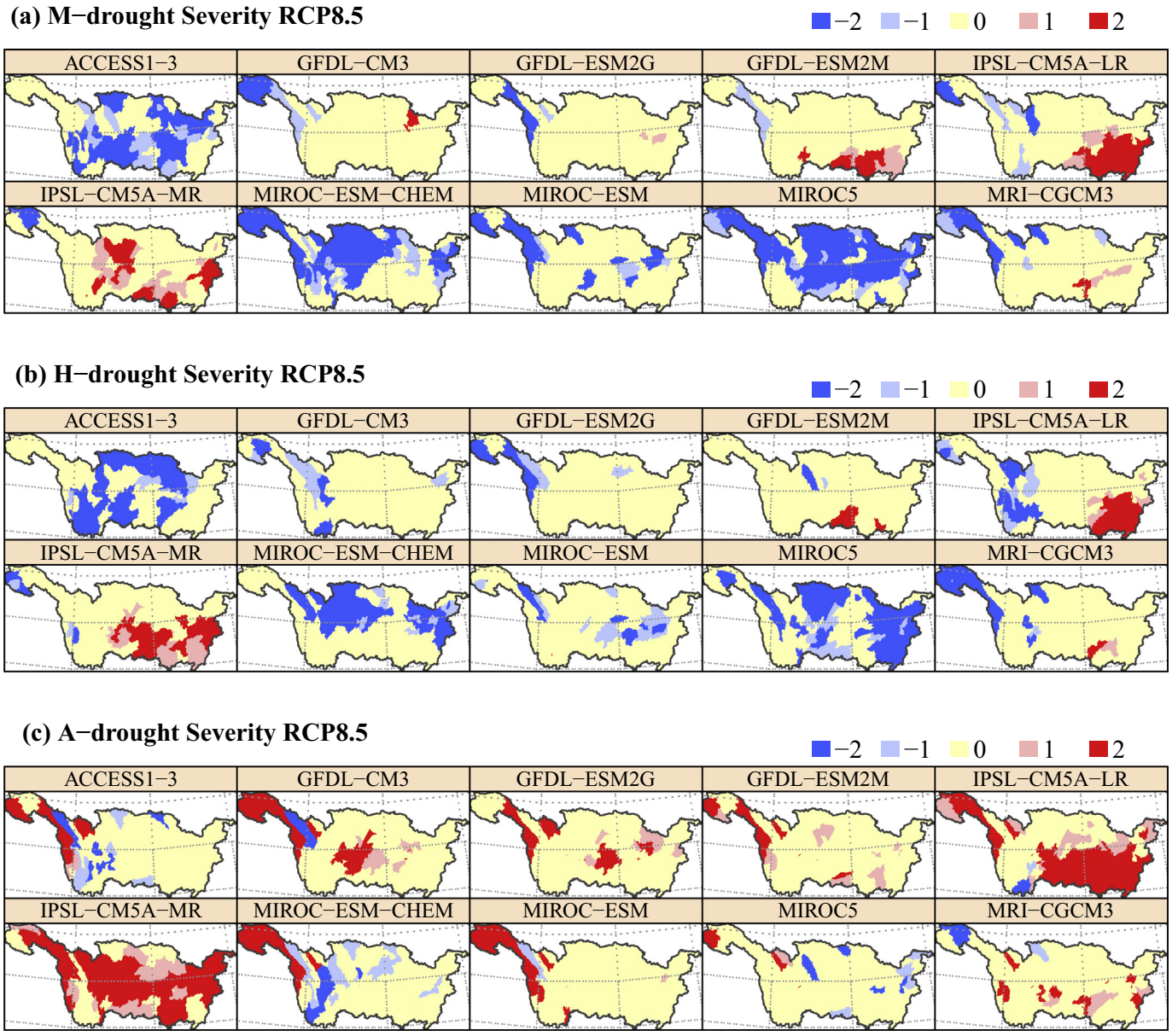

Fig. 10. As in Fig. 9 but for the RCP8.5 scenario.

is located in this region, which is one of China's fertile bread baskets (Xiang, 2014). A strong linear relationship between SSI values and agricultural production was reported by Kang et al. (2019). This region should be a priority to avoid future drought conditions having an adverse effect on its agricultural production. Moreover, we recommend that attention should be paid, in terms of drought monitoring and planning, to all the geographical areas revealing a projected drying of soil moisture so that mitigation actions can be taken before future drought conditions have a strong negative impact on those areas' socioeconomic activities and ecosystems.

6. Conclusions

This study projects future meteorological, hydrological, and agricultural droughts for the period 2021–2100 in the YRB, China. For this, precipitation and max/min temperatures from 10 CMIP5 climate models, under both the RCP4.5 and RCP8.5 emission scenarios, are spatially downscaled and bias-corrected to force the SWAT hydrological model. Projected runoff and soil moisture derived from the SWAT model outputs, along with bias-corrected precipitation, are used to characterize future H-drought, A-drought, and M-drought, respectively. Drought characteristics of severity, duration, frequency, and magnitude for the three drought types are analyzed and compared at the spatial scale of both the entire YRB and 125 subbasins. On the basis of our results, we emphasize the following conclusions:

The downscaled CMIP5 trends for the entire YRB over the projected period (2021–2100) indicate increasing precipitation, maximum temperature, and minimum temperature for both RCP4.5 and RCP8.5 scenarios. The increases tend to be larger for temperature than precipitation. These results highlight the need to analyze different drought variables, rather than relying solely on CMIP5 outputs, when assessing future drought conditions in the YRB, as the effects of increasing precipitation and temperature can counteract each other in terms of hydrological variables, e.g., soil moisture.

Projected precipitation and runoff for the entire YRB show a significant increasing trend for both RCP4.5 and RCP8.5 scenarios, with the majority of the CMIP5 models agreeing on the sign of the trend. In the case of soil moisture, the wetting trend tends to be weaker and less

consistent across the CMIP5 models. These results indicate that future hydrological conditions in the YRB are likely to have an unequal impact on different economic sectors. For example, the increasing runoff trend may be beneficial to hydroelectricity generation while the soil moisture trends suggest greater risks for agriculture.

The main effect of the projected CMIP5 precipitation and temperature outputs is to increase the magnitude and duration of the different drought types. Specifically, projected drought magnitudes in the YRB are anticipated to shift toward increasing severity as indicated by the increased frequency in extreme and exceptional droughts (D3 and D4) relative to the historical period. This increase in frequency is more severe for the A-drought (+10.4 occurrence times/decade) than the M- (+7.1 occurrence times/decade) and H-drought (+8.1 occurrence times/decade). Drought durations are also expected to increase for the projected period. These findings emphasize the need for water managers in the YRB to plan for worsening future drought conditions, despite the increasing trend in precipitation and runoff. Overall, the drought variables considered in the YRB respond differently to future drought conditions. In terms of frequency, precipitation is more sensitive in detecting droughts, or can capture the drought onset earlier than runoff and soil moisture. In terms of duration, runoff and soil moisture are more able to reliably capture drought persistence than precipitation. The different response of the drought variables highlights the importance of adopting suitable variables to inform different economic activities and sectors in the YRB.

The spatial pattern of future projected drought severity for the M-drought and H-drought reveals a largely non-significant trend in the majority of the subbasins. The remaining subbasins all show a decreasing trend. This is the case for both the RCP4.5 and RCP8.5 scenarios. The A-drought also shows mostly non-significant trends for both scenarios, but with a few areas revealing a generally increasing trend. These are geographical where special attention is needed to mitigate future drought impacts.

Acknowledgements

This study is supported by the National Key Research and Development Program of China (Grant No. 2017YFC0505701), and the Shanghai Key Lab for Urban Ecological Processes and Eco-Restoration (Grant No. SHUES2019B04).

References

AghaKouchak, A., 2014. A baseline probabilistic drought forecasting framework using standardized soil moisture index: application to the 2012 United States drought. Hydrol. Earth Syst. Sci. 18, 2485–2492.
Arnold, J.G., Srinivasan, R., Muttiah, R.S., Williams, J.R., 1998. Large Area Hydrologic Modeling and Assessment Part I: Model Development. Wiley Online Library.
Arnold, J.G., Moriasi, D.N., Gassman, P.W., Abbaspour, K.C., White, M.J., Srinivasan, R., et al., 2012. SWAT: model use, calibration, and validation. Trans. ASABE 55, 1491–1508.
Basheer, A.K., Lu, H.S., Omer, A., Ali, A.B., Abdelgader, A.M.S., 2016. Impacts of climate change under CMIP5 RCP scenarios on the streamflow in the Dinder River and ecosystem habitats in Dinder National Park, Sudan. Hydrol. Earth Syst. Sci. 20, 1331–1353.
Bisht, D.S., Sridhar, V., Mishra, A., Chatterjee, C., Raghuwanshi, N.S., 2019. Drought characterization over India under projected climate scenario. Int. J. Climatol. 39, 1889–1911.
Boé, J., Terray, L., Habets, F., Martin, E., 2007. Statistical and dynamical downscaling of the Seine basin climate for hydro-meteorological studies. Int. J. Climatol. 27, 1643–1655.
Cook, B.I., Ault, T.R., Smerdon, J.E., 2015. Unprecedented 21st century drought risk in the American Southwest and Central Plains. Sci. Adv. 1, e1400082.
Dai, A., 2011. Drought under global warming: a review. Wiley Interdiscip. Rev. Clim. Chang. 2, 45–65.
Deng, H., Luo, Y., Yao, Y., Liu, C., 2013. Spring and summer precipitation changes from 1880 to 2011 and the future projections from CMIP5 models in the Yangtze River Basin, China. Quat. Int. 304, 95–106.
Dracup, J.A., Lee, K.S., Paulson, E.G., 1980. On the definition of droughts. Water Resour. Res. 16, 297–302.
Entekhabi, D., Rodriguez-Iturbe, I., Castelli, F., 1996. Mutual interaction of soil moisture state and atmospheric processes. J. Hydrol. 184, 3–17.
FAO, 2014. World Reference Base for Soil Resources 2014. Food and Agriculture Orgnization of the United Nations.
Farahmand, A., AghaKouchak, A., 2015. A generalized framework for deriving nonparametric standardized drought indicators. Adv. Water Resour. 76, 140–145.
Gao, B., Yang, D., Zhao, T., Yang, H., 2012. Changes in the eco-flow metrics of the Upper Yangtze River from 1961 to 2008. J. Hydrol. 448–449, 30–38.
Gemmer, M., Jiang, T., Su, B., Kundzewicz, Z.W., 2008. Seasonal precipitation changes in the wet season and their influence on flood/drought hazards in the Yangtze River Basin, China. Quat. Int. 186, 12–21.
Girvetz, E.H., Maurer, E.P., Duffy, P.B., Ruesch, A., Thrasher, B., Zganjar, C., 2013. Making Climate Data Relevant to Decision Making: The Important Details of Spatial and Temporal Downscaling.
Griffin, D., Anchukaitis, K.J., 2014. How unusual is the 2012–2014 California drought? Geophys. Res. Lett. 41, 9017–9023.
Gringorten, I.I., 1963. A plotting rule for extreme probability paper. J. Geophys. Res. 68, 813–814.
Guan, Y., Zhang, X., Zheng, F., Wang, B., 2015. Trends and variability of daily temperature extremes during 1960-2012 in the Yangtze River Basin, China. Glob. Planet. Chang. 124, 79–94.
Gudmundsson, L., Bremnes, J.B., Haugen, J.E., Engen-Skaugen, T., 2012. Technical note: downscaling RCM precipitation to the station scale using quantile mapping–a comparison of methods. Hydrol. Earth Syst. Sci. 16, 3383–3390.
Guttman, N.B., 1999. Accepting the standardized precipitation index: a calculation algorithm. J. Am. Water Resour. Assoc. 35, 311–322.
Hao, Z., AghaKouchak, A., 2013. Multivariate standardized drought index: a parametric multi-index model. Adv. Water Resour. 57, 12–18.
Hao, Z., Singh, V., 2015. Drought characterization from a multivariate perspective: a review. J. Hydrol. 527, 668–678.
Heim, R.R., 2002. A review of twentieth-century drought indices used in the United States. Bull. Am. Meteorol. Soc. 83, 1149–1165.
Jakob Themeßl, M., Gobiet, A., Leuprecht, A., 2011. Empirical-statistical downscaling and error correction of daily precipitation from regional climate models. Int. J. Climatol. 31, 1530–1544.
Kang, H., Sridhar, V., 2017. Combined statistical and spatially distributed hydrological model for evaluating future drought indices in Virginia. J. Hydrol. Reg. Stud. 12, 253–272.
Kang, H., Sridhar, V., Mills, B.F., Hession, W.C., Ogejo, J.A., 2019. Economy-wide climate change impacts on green water droughts based on the hydrologic simulations. Agric. Syst. 171, 76–88.
Kendall, M.G., 1955. Rank Correlation Methods.
Kirtman, B., Power, S.B., Adedoyin, J.A., Boer, G.J., Bojariu, R., Camilloni, I., et al., 2013. Near-term climate change: Projections and predictability. In: Stocker, T.F., Qin, D., Plattner, G.-K., Tignor, M., Allen, S.K., Boschung, J., et al. (Eds.), Climate Change 2013: The Physical Science Basis. Contribution of Working Group I to the Fifth Assessment Report of the Intergovernmental Panel on Climate Change. Cambridge University Press, Cambridge, United Kingdom and New York, NY, USA, pp. 953–1028.
Leng, G., Tang, Q., Rayburg, S., 2015. Climate change impacts on meteorological, agricultural and hydrological droughts in China. Glob. Planet. Chang. 126, 23–34.
Lesk, C., Rowhani, P., Ramankutty, N., 2016. Influence of extreme weather disasters on global crop production. Nature 529, 84–87.
Liu, Y., Wu, G., Guo, R., Wan, R., 2016. Changing landscapes by damming: the Three Gorges Dam causes downstream lake shrinkage and severe droughts. Landsc. Ecol. 31, 1883–1890.
López-Moreno, J.I., Vicente-Serrano, S.M., Moran-Tejeda, E., Zabalza, J., Lorenzo-Lacruz, J., García-Ruiz, J.M., 2011. Impact of climate evolution and land use changes on water yield in the Ebro basin. Hydrol. Earth Syst. Sci. 15, 311–322.
Lu, E., Luo, Y., Zhang, R., Wu, Q., Liu, L., 2011. Regional atmospheric anomalies responsible for the 2009–2010 severe drought in China. J. Geophys. Res.-Atmos. 116.
Lu, G., Wu, H., Xiao, H., He, H., Wu, Z., 2016. Impact of climate change on drought in the upstream Yangtze River region. Water 8, 576.
Mann, H.B., 1945. Nonparametric tests against trend. Econometrica 245–259.
Maraun, D., 2016. Bias correcting climate change simulations - a critical review. Curr. Clim. Chang. Rep. 2, 211–220.
McKee, T.B., Doesken, N.J., Kleist, J., 1993. The relationship of drought frequency and duration to time scales. Proceedings of the 8th Conference on Applied Climatology. 17, pp. 179–183.
Mishra, A., Singh, V., 2010. A review of drought concepts. J. Hydrol. 391, 202–216.
Mo, K.C., 2011. Drought onset and recovery over the United States. J. Geophys. Res.-Atmos. 116.
Moss, R.H., Edmonds, J.A., Hibbard, K.A., Manning, M.R., Rose, S.K., van Vuuren, D.P., et al., 2010. The next generation of scenarios for climate change research and assessment. Nature 463, 747–756.
Nasrollahi, N., AghaKouchak, A., Cheng, L., Damberg, L., Phillips, T.J., Miao, C., et al., 2015. How well do CMIP5 climate simulations replicate historical trends and patterns of meteorological droughts? Water Resour. Res. 51, 2847–2864.
Nazareno, A.G., Laurance, W.F., 2015. Brazil's drought: beware deforestation. Science 347, 1427.
Orlowsky, B., Seneviratne, S.I., 2013. Elusive drought: uncertainty in observed trends and short- and long-term CMIP5 projections. Hydrol. Earth Syst. Sci. 17, 1765–1781.
Pan, Z., Zhang, Y., Liu, X., Gao, Z., 2016. Current and future precipitation extremes over Mississippi and Yangtze River basins as simulated in CMIP5 models. J. Earth Sci. 27, 22–36.
Rajsekhar, D., Gorelick, S.M., 2017. Increasing drought in Jordan: climate change and cascading Syrian land-use impacts on reducing transboundary flow. Sci. Adv. 3, e1700581.
Schwalm, C.R., Anderegg, W.R.L., Michalak, A.M., Fisher, J.B., Biondi, F., Koch, G., et al., 2017. Global patterns of drought recovery. Nature 548, 202–205.
Sehgal, V., Sridhar, V., 2018. Effect of hydroclimatological teleconnections on the watershed-scale drought predictability in the southeastern United States. Int. J. Climatol. 38, e1139–e1157.

Sehgal, V., Sridhar, V., 2019. Watershed-scale retrospective drought analysis and seasonal forecasting using multi-layer, high-resolution simulated soil moisture for Southeastern US. Weather Clim. Extremes 23, 100191.
Sehgal, V., Sridhar, V., Tyagi, A., 2017. Stratified drought analysis using a stochastic ensemble of simulated and in-situ soil moisture observations. J. Hydrol. 545, 226–250.
Sehgal, V., Sridhar, V., Juran, L., Ogejo, J., 2018. Integrating climate forecasts with the soil and water assessment tool (SWAT) for high-resolution hydrologic simulations and forecasts in the southeastern US. Sustainability 10, 3079.
Sheffield, J., Wood, E.F., Roderick, M.L., 2012. Little change in global drought over the past 60 years. Nature 491, 435–438.
Shrestha, N.K., Du, X., Wang, J., 2017. Assessing climate change impacts on fresh water resources of the Athabasca River Basin, Canada. Sci. Total Environ. 601–602, 425–440.
Shukla, S., Wood, A.W., 2008. Use of a standardized runoff index for characterizing hydrologic drought. Geophys. Res. Lett. 35.
Song, L., Deng, Z., Dong, A., 2003. Global Change in Arid Hot Topics. China Meteorological Press, Beijing.
Sun, F., Kuang, W., Xiang, W., Che, Y., 2016. Mapping water vulnerability of the Yangtze River Basin: 1994–2013. Environ. Manag. 58, 857–872.
Svoboda, M., LeComte, D., Hayes, M., Heim, R., Gleason, K., Angel, J., et al., 2002. The drought monitor. Bull. Am. Meteorol. Soc. 83, 1181–1190.
Tan, M.L., Ibrahim, A., Yusop, Z., Chua, V.P., Chan, N.W., 2017. Climate change impacts under CMIP5 RCP scenarios on water resources of the Kelantan River Basin, Malaysia. Atmos. Res. 189 (1–10).
Taylor, K.E., Stouffer, R.J., Meehl, G.A., 2012. An overview of CMIP5 and the experiment design. Bull. Am. Meteorol. Soc. 93, 485–498.
Teutschbein, C., Seibert, J., 2012. Bias correction of regional climate model simulations for hydrological climate-change impact studies: review and evaluation of different methods. J. Hydrol. 456-457, 12–29.
Thilakarathne, M., Sridhar, V., 2017. Characterization of future drought conditions in the Lower Mekong River Basin. Weather Clim. Extremes 17, 47–58.
Thrasher, B., Maurer, E.P., McKellar, C., Duffy, P.B., 2012. Bias correcting climate model simulated daily temperature extremes with quantile mapping. Hydrol. Earth Syst. Sci. 16, 3309–3314.
Touma, D., Ashfaq, M., Nayak, M., Kao, S.-C., Diffenbaugh, N., 2015. A multi-model and multi-index evaluation of drought characteristics in the 21st century. J. Hydrol. 526, 196–207.
Van Dijk, A.I.J.M., Beck, H.E., Crosbie, R.S., Jeu, R.A.M., Liu, Y.Y., Podger, G.M., et al., 2013. The millennium drought in southeast Australia (2001–2009): natural and human causes and implications for water resources, ecosystems, economy, and society. Water Resour. Res. 49, 1040–1057.
Venkataraman, K., Tummuri, S., Medina, A., Perry, J., 2016. 21st century drought outlook for major climate divisions of Texas based on CMIP5 multimodel ensemble: implications for water resource management. J. Hydrol. 534, 300–316.
Vicca, S., Balzarolo, M., Filella, I., Granier, A., Herbst, M., Knohl, A., et al., 2016. Remotely-sensed detection of effects of extreme droughts on gross primary production. Sci. Rep. 6, 28269.
Vicente-Serrano, S.M., Beguería, S., López-Moreno, J.I., 2010. A multiscalar drought index sensitive to global warming: the standardized precipitation evapotranspiration index. J. Clim. 23, 1696–1718.
Vicente-Serrano, S.M., Begueria, S., Lopez-Moreno, J.I., 2011. Comment on "Characteristics and trends in various forms of the Palmer Drought Severity Index (PDSI) during 1900-2008" by Aiguo Dai. J. Geophys. Res.-Atmos. 116.
Wang, L., Chen, W., 2014. A CMIP5 multimodel projection of future temperature, precipitation, and climatological drought in China. Int. J. Climatol. 34, 2059–2078.
Wang, A., Lettenmaier, D.P., Sheffield, J., 2011. Soil moisture drought in China, 1950–2006. J. Clim. 24, 3257–3271.
Westmacott, J., Burn, D., 1997. Climate change effects on the hydrologic regime within the Churchill-Nelson River Basin. J. Hydrol. 202, 263–279.
Wilhite, D.A., Glantz, M.H., 1985. Understanding: the drought phenomenon: the role of definitions. Water Int. 10, 111–120.
Wood, A.W., Maurer, E.P., Kumar, A., Lettenmaier, D.P., 2002. Long-range experimental hydrologic forecasting for the eastern United States. J. Geophys. Res.-Atmos. ACL-6, 107.
Wood, A.W., Leung, L.R., Sridhar, V., Lettenmaier, D.P., 2004. Hydrologic implications of dynamical and statistical approaches to downscaling climate model outputs. Clim. Chang. 62, 189–216.
World Economic Forum, 2017. The Global Risks Report 2017.
Wu, Y., Wu, S., Wen, J., Tagle, F., Xu, M., Tang, J., 2016. Future changes in mean and extreme monsoon precipitation in the Middle and Lower Yangtze River Basin, China, in the CMIP5 models. J. Hydrometeorol. 17, 2785–2797.
Xiang, W.-N., 2014. Doing real and permanent good in landscape and urban planning: ecological wisdom for urban sustainability. Landsc. Urban Plan. 121, 65–69.
Xu, K., Yang, D., Yang, H., Li, Z., Qin, Y., Shen, Y., 2015. Spatio-temporal variation of drought in China during 1961–2012: a climatic perspective. J. Hydrol. 526, 253–264.
Yang, J., Gong, D., Wang, W., Hu, M., Mao, R., 2012. Extreme drought event of 2009/2010 over southwestern China. Meteorog. Atmos. Phys. 115, 173–184.
Zhai, J., Su, B., Krysanova, V., Vetter, T., Gao, C., Jiang, T., 2010. Spatial variation and trends in PDSI and SPI indices and their relation to streamflow in 10 large regions of China. J. Clim. 23, 649–663.
Zhou, L., Wu, J., Mo, X., Zhou, H., Diao, C., Wang, Q., et al., 2017. Quantitative and detailed spatiotemporal patterns of drought in China during 2001-2013. Sci. Total Environ. 589, 136–145.
Zhu, Y., Wang, W., Singh, V.P., Liu, Y., 2016. Combined use of meteorological drought indices at multi-time scales for improving hydrological drought detection. Sci. Total Environ. 571, 1058–1068.
Zou, X., Zhai, P., Zhang, Q., 2005. Variations in droughts over China: 1951–2003. Geophys. Res. Lett. 32.